# K Improves Cu(In,Ga)Se$_2$ Surface Band Alignment through Reconstruction

Christopher P. Muzzillo,* Stephen Glynn, Glenn Teeter, and Lorelle M. Mansfield

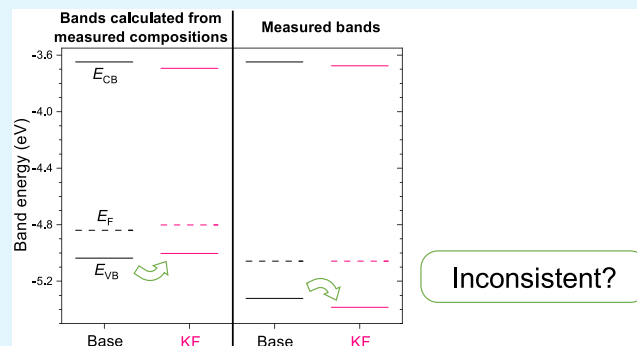Cite This: *ACS Appl. Energy Mater.* 2022, 5, 11328−11338

Read Online

ACCESS | Metrics & More | Article Recommendations

**ABSTRACT:** K, Rb, and Cs improve Cu(In,Ga)Se$_2$ (CIGS) solar cell performance, but the mechanism remains unclear. Here we use air-free transfer of multiple samples to study KF post-deposition treatments (PDTs) by X-ray photoelectron spectroscopy. The KF PDTs do not change the majority carrier concentration or Cd in-diffusion, but they boost efficiency by 6.1% absolute, improve minority carrier lifetime, and shift the surface valence band further from the Fermi energy. Unlike former reports, the valence-band shift is not a result of lower Cu/(Ga+In) or higher K/(K+Cu) composition ratios. We propose that instead, KF PDTs alter the surface valence-band alignment through a reconstructive phase transformation from chalcopyrite CIGS to K$_2$CuIn$_3$Se$_6$ or KInSe$_2$, which have layered structures. These compounds can leave Cu-free cation planes after K is rinsed away, unlike the structure of chalcopyrite CIGS or CuIn$_3$Se$_5$.



**KEYWORDS:** CIGS, chalcopyrite, potassium, reconstruction, photovoltaics

## INTRODUCTION

Since 2013, the introduction of K, Rb, or Cs has advanced the photovoltaic (PV) conversion efficiency of Cu(In,Ga)(Se,S)$_2$ (CIGS) from 20.3 to 23.4%. Eight of the last ten world record cells used KF,[1−4] RbF,[5,6] or CsF.[7,8] In the decades prior to that, the role of Na in CIGS devices was well studied,[9−11] but from the outset,[1] KF, RbF, and CsF postdeposition treatments (PDTs) exhibited effects that are a departure from Na. In particular, alkali fluorides react with the CIGS surface, altering its chemical composition. KInSe$_2$, RbInSe$_2$, and CsInSe$_2$ have two-dimensional (2D) monoclinic structures and are more stable than NaInSe$_2$, the latter of which has the three-dimensional (3D) chalcopyrite structure.[12] RbInSe$_2$ and CsInSe$_2$ were both directly observed at the surface of CIGS absorbers in efficient devices,[13−16] and form a 3D/2D chalcopyrite/monoclinic interface hypothesized to passivate dangling bonds.[17] Although it has not been directly observed, extensive indirect evidence was compiled that indicates KInSe$_2$ also passivates high efficiency CIGS.[18−20]

First-principles calculations predict that K and Rb are too large to incorporate into CIGS grains, making their defect formation energies infeasibly high.[12,21−25] On the other hand, K has been directly observed within Cu-poor CuInSe$_2$ grains[26] and within epitaxial CIGS crystals.[27,28] Rb was also found to diffuse into CIGS grains.[29] Therefore, the experimental evidence still holds that grain interior, grain boundary and interface effects should be considered to understand K and
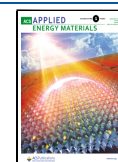
Rb,[30] although no evidence of Cs on grain interiors has been reported yet. We note that theory[12,23] and experiment[27] qualitatively agree that Cu-poor compositions facilitate the incorporation and diffusion of heavy alkali metals relative to Cu-rich material.

In light of the complex effects of the heavy alkali metals, many investigations have sought to characterize the surface composition and band alignment of KF-, RbF-, and CsF-treated CIGS using X-ray photoelectron spectroscopy (XPS) and related techniques. After a KF PDT, as deposited surfaces typically exhibit reduced Cu content,[31−38] although no change to Cu has been reported.[39] These surfaces simultaneously show decreased Ga[31,35,37] or increased In,[31] but increased Ga[34] and decreased In[35] have also been observed. Even samples that receive K before or during absorber growth have less Cu[40,41] or more In[42] on their as deposited surfaces. Since the majority of absorbers undergo chemical bath deposition (CBD) of CdS or Zn(O,S,OH) buffers, a more device-relevant surface is prepared by rinsing the CIGS in NH$_3$ or deionized (DI) water before characterization. Rinsed surfaces also reveal that

KF PDTs reduce Cu,[1,33,43−51] reduce Ga,[1,33,43,47,51] and increase In,[43,47] although no effect on Cu,[52] increased Cu,[49,53] and increased Ga[44] have been reported. Similarly, Ar+ sputter-cleaning the CIGS surface shows that KF PDTs decrease Cu,[54−56] decrease Ga,[56] and increase In,[54] but increased Ga[54] was also reported. Bringing the CIGS surface one step closer to its state in the final device, researchers have also dipped samples in $Cd^{2+}$ solutions or deposited thin buffers, after which the KF PDT samples had decreased Cu,[57,58] decreased Ga,[57,58] and increased Cd.[37,57,58] In summary, despite variations in findings that may stem from metal halide, oxide, and hydroxide formation and dissolution, K has a chemical affinity for In that causes KF PDTs to reduce surface Cu and Ga content.

Concomitant with these compositional alterations, rinsed CIGS surfaces show valence band energies (relative to the Fermi energy; $E_F − E_{VB}$) after KF PDTs that are changed by −0.12 eV to −1.15 eV (Table 1). Ex situ KF PDTs and adding

**Table 1. Literature Surface Band Energy Shifts Associated with KF, RbF, and CsF PDTs**

| process | $E_{VB}$ shift (eV) | $E_{CB}$ shift (eV) | $E_g$ shift (eV) | ref |
|---|---|---|---|---|
| KF PDT | −0.37 | | | [50] |
| | −0.12 to −0.15 | | | [67] |
| | −0.60 | +0.39 | +0.99 | [18] |
| | −0.16 | +0.25 | +0.41 | [59] |
| | −1.15 | −0.06 | +1.09 | [48] |
| | −0.19 | | | [68] |
| | −0.18 | | | [69] |
| | −0.17 | −0.14 | −0.03 | [51] |
| | −0.57 | −0.03 | +0.54 | [60] |
| KI PDT | −0.18 | | | [56] |
| ex situ KF PDT | +0.48 to +1.36 | | | [49] |
| KF during selenization | +0.15 | | | [42] |
| RbF PDT | −0.17 | −0.12 | +0.05 | [70] |
| | −0.16 to −0.26 | | | [71] |
| | −0.30 | −0.25 | +0.05 | [60] |
| CsF PDT | −0.10 to −0.25 | | | [72,73] |

KF during selenization can lead to increased valence band energy, but decreased valence band energy is the prevailing observation. The conduction band energy (relative to the Fermi energy; $E_{CB} − E_F$) associated with KF is altered by −0.06 eV to +0.39 eV (Table 1). These conduction band changes with KF PDTs were associated with surface band gap widening from 1.69 to 2.68 eV,[18] from 1.82 to 2.23 eV,[59] from 1.46 to 2.00 eV,[60] and from 1.30 to 2.39 eV,[48] ($E_g = E_{CB} − E_{VB}$). Compounds with relevant band gaps include $KInSe_2$ with 2.68 eV,[61] $K_2In_{12}Se_{19}$ with 2.25 eV,[62] $K_{0.67}Cu_{0.33}InSe_2$ (or $K_2CuIn_3Se_6$) with 1.60 to 1.72 eV,[63−65] $K_{0.67}Cu_{0.33}GaSe_2$ with 1.72 eV,[63] and $KIn_{0.43}Ga_{0.57}Se_2$ with 2.77 eV.[66] In summary, KF PDTs reduce the surface valence band energy and are usually associated with band gap widening, but attributing these changes to a single K-containing compound is difficult, particularly since K is not always detected on the surface.[44,47,55]

RbF PDTs generally exhibit analogous behavior to K: Cu is reduced,[71,74−82] Ga is reduced,[71,74,75,77−82] and In is increased,[74,79] although unchanged Ga,[76] increased Ga,[80,81] and decreased In[77] have been found. RbF PDTs are associated with valence band energy changes of −0.16 eV to −0.30 eV (Table 1). The conduction band energy resulting from an RbF

PDT changed by −0.12 eV to −0.25 eV, corresponding to band gap widening from 1.46 to 1.51 eV.[60,70] CsF PDTs also reduce Cu,[72,73,78,83] reduce Ga,[72,73,78] and alter $E_{VB}$ by −0.1 to −0.25 eV (Table 1). In summary, KF, RbF and CsF all exhibit analogous behavior by reducing surface Cu, Ga, and valence band energy, but results are consistently inconsistent.

In this study, we utilize air-free transfer methods to characterize the effects of KF PDTs. We study multiple samples to improve the statistical robustness of the results. Our KF PDTs boost efficiency by 6.1% absolute. The data suggest that this improvement is dominated by a reduction in recombination and surface valence band, but the valence band reduction occurs in the absence of changes to surface Cu or K composition. To explain this and other confounding literature results, we propose that KF PDTs reconstruct CIGS surfaces, forming weakly bound Cu-free planes that persist in reducing the valence band even after K is rinsed away.

## EXPERIMENTAL SECTION

We coat soda-lime glass (SLG) substrates with 800 nm of DC sputtered Mo. We then load 3 in. × 3 in. substrates into a cluster tool with a co-evaporation growth chamber with Cu, In, Ga, and KF effusion sources, along with a valved tank source for Se. We grow baseline CIGS absorbers with ∼2.7 µm thickness by three-stage co-evaporation at 575 °C. The KF PDT consists of cooling the substrate to 380 °C and evaporating KF at 0.1 nm/s (source at 660 °C) for 7.5 min with Se overpressure. Next, we robotically transfer the samples under vacuum into a mobile pod attachment, after which they are vented to an $N_2$ atmosphere and diced into pieces in a glovebox with <0.1 ppm of $H_2O$ and $O_2$. For characterization of the "as deposited" surfaces, we load pieces into a Physical Electronics Phi 5000 VersaProbe III system for XPS and low-energy inverse photoemission spectroscopy (LEIPS) without air exposure. High-resolution XPS spectra are acquired at 26 eV pass energy, with X-ray anode power = 24.5 W, and rastered analysis areas of $(100 \ \mu m)^2$. LEIPS measurements are performed with low-energy electron excitation (10 eV incident energy, 3 µA beam current) and emitted photons are passed through a bandpass filter (central wavelength = 250 nm, width = 20 nm). Some samples' In core levels shifted when the LEIPS working bias was applied, so we subtract that shift from the as-measured LEIPS binding energies. Next, we expose these same pieces to air for 15 min and load them back into the XPS chamber. Finally, we rinse these pieces in a 3% (w/w) aqueous $NH_3$ solution for 4 min in a jacketed beaker with water circulating at 65 °C, followed by directly immersing in deionized (DI) water. We then transfer the immersed samples into a glovebox, blow them dry with $N_2$, and load them back into the XPS chamber without air exposure.

We cut separate pieces from these samples to fabricate solar cells by using the same $NH_3$ rinse procedure, followed by CBD of ∼50 nm CdS, RF sputtering of 90 nm i-ZnO, 120 nm Al:ZnO, evaporation of Ni/Al grids, and isolation of 0.42 $cm^2$ cells by photolithography and etching. We perform current density−voltage ($JV$) measurements on a temperature-controlled stage set to 25 °C under xenon bulb illumination calibrated to 1 sun AM1.5G with a standard Si solar cell. We measure capacitance−voltage ($CV$) at room temperature in the dark at 10 kHz and 50 mV AC voltage, with DC bias swept from +0.6 V to −1.5 V, and calculate carrier concentration assuming a dielectric constant of 13.6.

We confirm overall absorber composition to have Cu/(Ga+In) ∼ 0.85 and Ga/(Ga+In) ∼ 0.3 by X-ray fluorescence. We perform secondary ion mass spectrometry (SIMS) on device stacks using $Cs^+$ ions to validate that the relative Cu, Ga and In composition profiles are consistent for all six samples grown in this study. The SIMS data are scaled so that all samples' ZnO thicknesses match. We additionally measure absolute Na and K composition profiles by SIMS using calibration standards. We perform time-resolved photoluminescence (TRPL) on bare absorbers at 1 MHz with a 50 µm spot size and a 670 nm laser at $6.9 \cdot 10^{17}$ photons $cm^{−2} \ s^{−1}$ (205 nJ $cm^{−2}$ per pulse). We

**Table 2. Sample Designation, Mean Efficiency, Open-Circuit Voltage ($V_{OC}$), Short-Circuit Current Density ($J_{SC}$), Fill Factor (FF), Carrier Concentration from CV, Integral Absorber Na and K Concentration from SIMS, Long Component of the Minority Carrier Lifetime ($\tau_2$) from TRPL, NH$_3$ Rinsed Valence Band Energy Relative to Fermi Energy ($E_F - E_{VB}$) from XPS, NH$_3$ Rinsed Conduction Band Energy Relative to Fermi Energy ($E_{CB} - E_F$) from LEIPS, and NH$_3$ Rinsed Band Gap ($E_g$) from LEIPS and XPS[a]**

| sample | eff. (%) | $V_{OC}$ (mV) | $J_{SC}$ (mA/cm$^2$) | FF (%) | $p$ ($\times 10^{15}$ cm$^{-3}$) | Na ($\times 10^{18}$ cm$^{-3}$) | K ($\times 10^{18}$ cm$^{-3}$) | $\tau_2$ (ns) | $E_F - E_{VB}$ (eV) | $E_{CB} - E_F$ (eV) | $E_g$ (eV) |
|---|---|---|---|---|---|---|---|---|---|---|---|
| Base-1 | 9.9(7) | 603(15) | 34.8(7) | 47.3(25) | 8.1(12) | 9.6 | 1.3 | 36 | −0.31 | 1.31 | 1.62 |
| Base-2 | 7.2(16) | 555(8) | 31.6(21) | 40.6(71) | 4.0(3) | 11 | 1.5 | 25 | −0.22 | 1.40 | 1.62 |
| Base-3 | 6.3(6) | 631(2) | 25.6(47) | 39.8(37) | 8.5(6) | 7.3 | 1.4 | 59 | −0.26 | 1.52 | 1.78 |
| KF-1 | 13.3(3) | 614(3) | 35.1(2) | 61.6(8) | 10.4(5) | 5.7 | 13 | 79 | −0.36 | 1.52 | 1.88 |
| KF-2 | 13.6(7) | 619(5) | 34.1(5) | 64.2(23) | 4.8(2) | 6.0 | 12 | 58 | −0.35 | 1.32 | 1.67 |
| KF-3 | 14.6(4) | 602(7) | 35.3(1) | 68.7(10) | 4.4(2) | 6.8 | 11 | 73 | −0.27 | 1.31 | 1.58 |
| All base | 7.7(18) | 597(34) | 30.4(49) | 42.3(58) | 6.8(22) | 9.2(17) | 1.4(1) | 40(16) | −0.26(5) | 1.41(11) | 1.67(9) |
| All KF | 13.8(7) | 612(9) | 34.7(6) | 64.9(32) | 6.6(29) | 6.2(6) | 12(1) | 70(10) | −0.33(5) | 1.38(12) | 1.71(15) |

[a]Standard deviations are in parentheses.

measure TRPL at multiple locations for each sample to verify uniformity and fit the data to biexponential functions to extract short and long lifetimes ($\tau_1$ and $\tau_2$, respectively).

## RESULTS

To ensure that the results for this study are reproducible, we grow three baseline and three KF PDT films. Table 2 has a summary of the PV parameters for each, showing that the KF PDT increases efficiency by 79%, relative to the baselines, which is dominated by a 53% fill factor boost. The cluster tool growth chamber produces lower efficiency CIGS than NREL's other co-evaporation systems, possibly because of its Se source-to-substrate distance, which is 3× further and limits Se flux. SIMS confirms that KF PDTs increase the integral absorber K concentration from $1.5 \times 10^{18}$ cm$^{-3}$ to $1.8 \times 10^{19}$ cm$^{-3}$. The KF PDT is also associated with a slight decrease in Na by SIMS. The carrier concentration by CV for all samples is similar, indicating that unlike Na, K's beneficial effects do not stem from its role as a p-type dopant.

The samples all have similar looking TRPL data (Figure 1). Fitting the TRPL data to biexponential functions yields similar
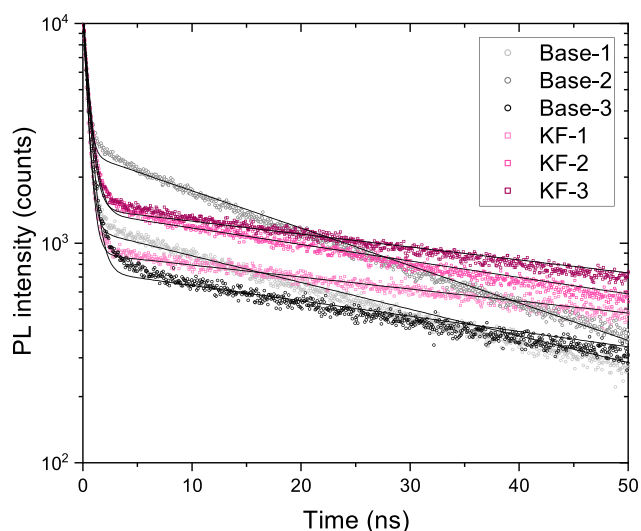


**Figure 1.** TRPL for the 6 samples in this study: Base-1 (light gray), Base-2 (gray), Base-3 (black), KF-1 (light pink), KF-2 (pink), and KF-3 (dark pink). The KF samples mostly have moderately superior lifetimes.

short components of the minority carrier lifetimes ($\tau_1$): 0.42(10) and 0.48(7) ns for the baseline and KF PDT samples, respectively. On the other hand, Table 2 shows that the long component of the lifetime ($\tau_2$) improves by 75% for the KF PDT samples. Although traps and band gap gradients convolute the TRPL data, a straightforward interpretation is that KF PDTs reduce non-radiative recombination in the bulk absorber. On the other hand, the Base-3 sample has a $\tau_2$ of 59 ns and 6.3% efficiency, while the KF-2 sample has a $\tau_2$ of 58 ns and 13.6% efficiency. Simulations using the baseline graded CIGS device model that comes bundled with wxAMPS version 2[84,85] require a 10× increase in bulk electron lifetime (from 0.5 to 5 ns) in order to boost efficiency from 7.7 to 15.5%. Since experiments achieved a comparable efficiency increase with only 1.75× higher lifetimes, we conclude that for this study, KF PDT bulk passivation is not the primary mechanism of PV performance enhancement.

Since the KF PDT advances efficiency, but not through doping or bulk passivation, we characterize the CIGS surfaces with XPS. We perform XPS before the absorbers are exposed to air, after they are exposed to air, and after an NH$_3$ rinse. Figure 2a shows that the vacuum transfer process leads to negligible oxidation of the surfaces and that the NH$_3$ rinse successfully removes the oxides that form after air exposure. Figure 2b shows that the as deposited and air exposed KF PDT samples have fluoride compounds (Ga−F, Na−F, and K−F) that must be rinsed away (along with the oxides) for band energy data to be attributable to the device-relevant semi-conductors. Figure 2c shows that the NH$_3$ rinse also tends to reduce K to below the detection limit for XPS, although SIMS on devices shows that 0.1−0.3% (v/v) K is retained at the CIGS/CdS interface. Figure 2d shows that the baseline samples have Na on their surfaces, and the KF PDT samples have increased Na.

We examine the NH$_3$ rinsed XPS data in more detail in Figure 3 and find that Base-1 has slightly less Cu and KF-2 has significantly less Cu, but otherwise the samples have similar Cu peaks. On the other hand, the KF PDT clearly reduces Ga in Figure 3b, possibly through the formation of some soluble gallium compound that is rinsed away. The KF-2 sample also shows less In, while all other samples have similar In peaks in Figure 3c. Quantitative XPS compositions of the NH$_3$ rinsed samples are in Table 3, showing that the KF PDT is associated with increased K, Cu, In, and Se, as well as decreased Ga. The
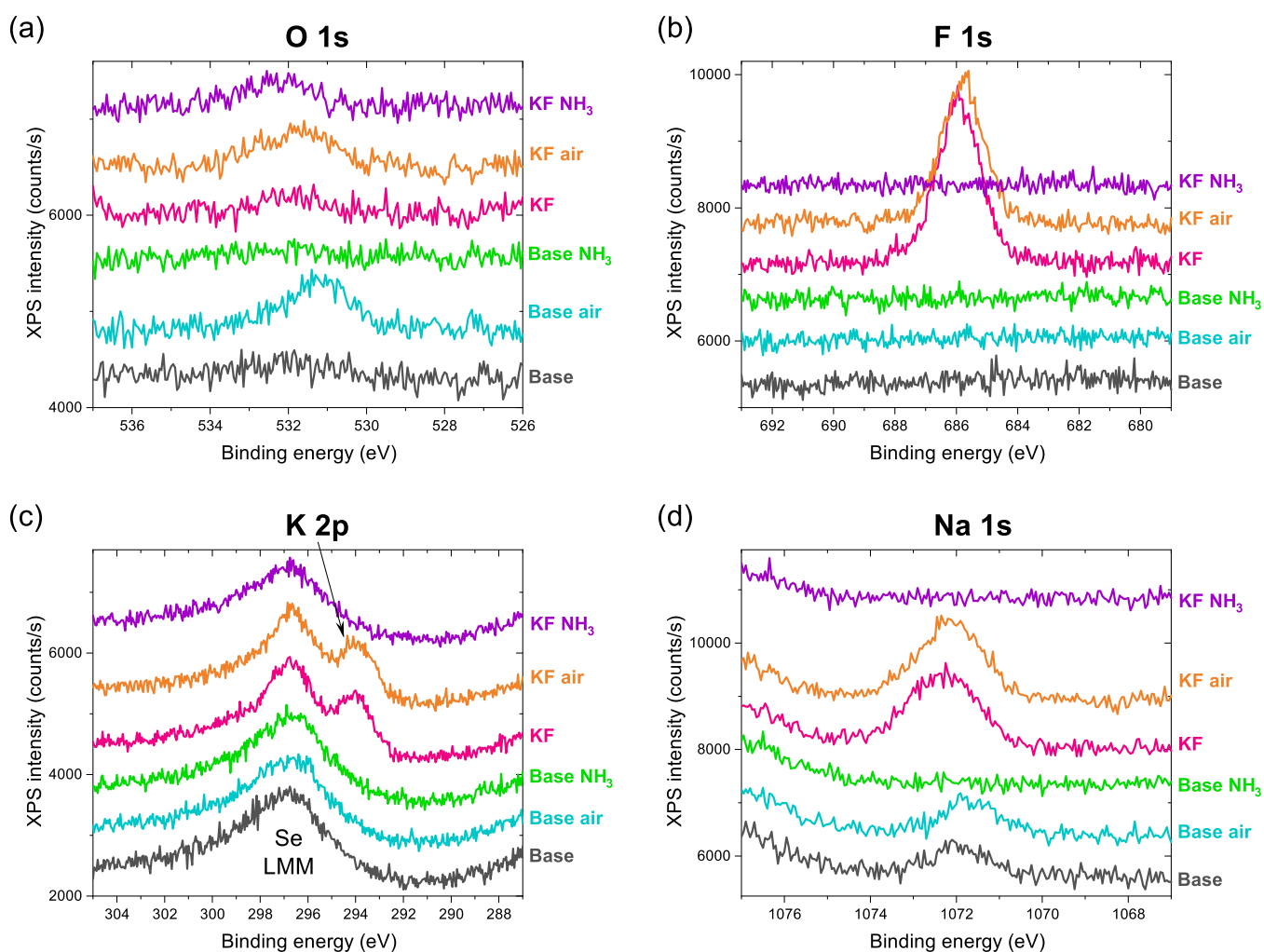
**Figure 2.** XPS detailed spectra of the (a) O 1s, (b) F 1s, (c) K 2p, and (d) Na 1s peaks for the as deposited (gray), air exposed (light blue), and NH$_3$ rinsed (green) Base-2 sample, as well as the as deposited (pink), air exposed (orange), and NH$_3$ rinsed (purple) KF-2 sample.

results in Table 3 use the tabulated standard sensitivity factors and inelastic mean free paths for quantifying composition. We also correct sensitivity factors and inelastic mean free paths to depend on composition, which slightly changes the results (Table 4). The correction increases Cu while decreasing In and Ga, while also increasing Cu's standard deviation. Overall we conclude from Tables 3 and 4 that the PDT reduced Ga and did not significantly change Cu or K.

The decrease in Ga correlates with a slight decrease in conduction band energy (Figure 3d, right axis; Table 2). Small changes in surface Ga/(Ga+In) composition generally just shift the $V_{OC}$–$J_{SC}$ trade-off,[86] so we do not attribute the KF PDT's FF boost to Ga or $E_{CB}$ reduction. On the other hand, despite the KF PDT not significantly changing Cu/(Ga+In) and K/(K+Cu), there is a concomitant reduction in valence band energy (Figure 3d left axis; Table 2). Similar downward $E_{VB}$ shifts were reported in all 10 KF (or KI) PDT studies where $E_{VB}$ was measured (Table 1).

We note that surface band gaps in Table 2 are wider than expected from bulk film compositions, which is commonly observed with XPS on similar films.[18,51,59,60,70] Downward surface band bending, Fermi level pinning, and X-ray quasi-Fermi level splitting all complicate the interpretation of XPS and LEIPS band edge measurements. The PDT's association with band gap widening in spite of Ga/(Ga+In) reduction indicates that the band shifts are not a result of band bending or Fermi pinning. Instead, the band data should result from changes to the material's band structure. In Figure 4 we compare the measured band energies to band energies calculated from the measured compositions in Table 3 (assuming both baseline cases have electron affinity = 3.56 eV and band offsets depend on Cu/(Ga+In) and Ga/(Ga+In) composition[87]). The straightforward interpretation of Figure 4 is that the band and composition trends are inconsistent.

Former studies have found that KF and RbF PDTs enhance the nucleation of CdS and the diffusion of Cd into the absorber, both of which were posited to benefit the quality of the homojunction.[1,37,57,58,74,88] For instance, the monoclinic 2D compound CsInSe$_2$ was hypothesized to incorporate Cd and S to form the 2D compound CsCdInSe$_3$,[89] or cation and anion exchange may transform KInSe$_2$ into CdIn$_2$S$_4$.[30,37,90,91] We perform SIMS on the full device stack to compare Cd in-diffusion of the samples. Figure 5 shows that the Cd profiles are indistinguishable. Whereas the SIMS data do not rule out greater n-type Cd doping of the KF PDT surfaces, we find no evidence that the KF PDT benefits hinge upon CBD changes.

## ■ DISCUSSION

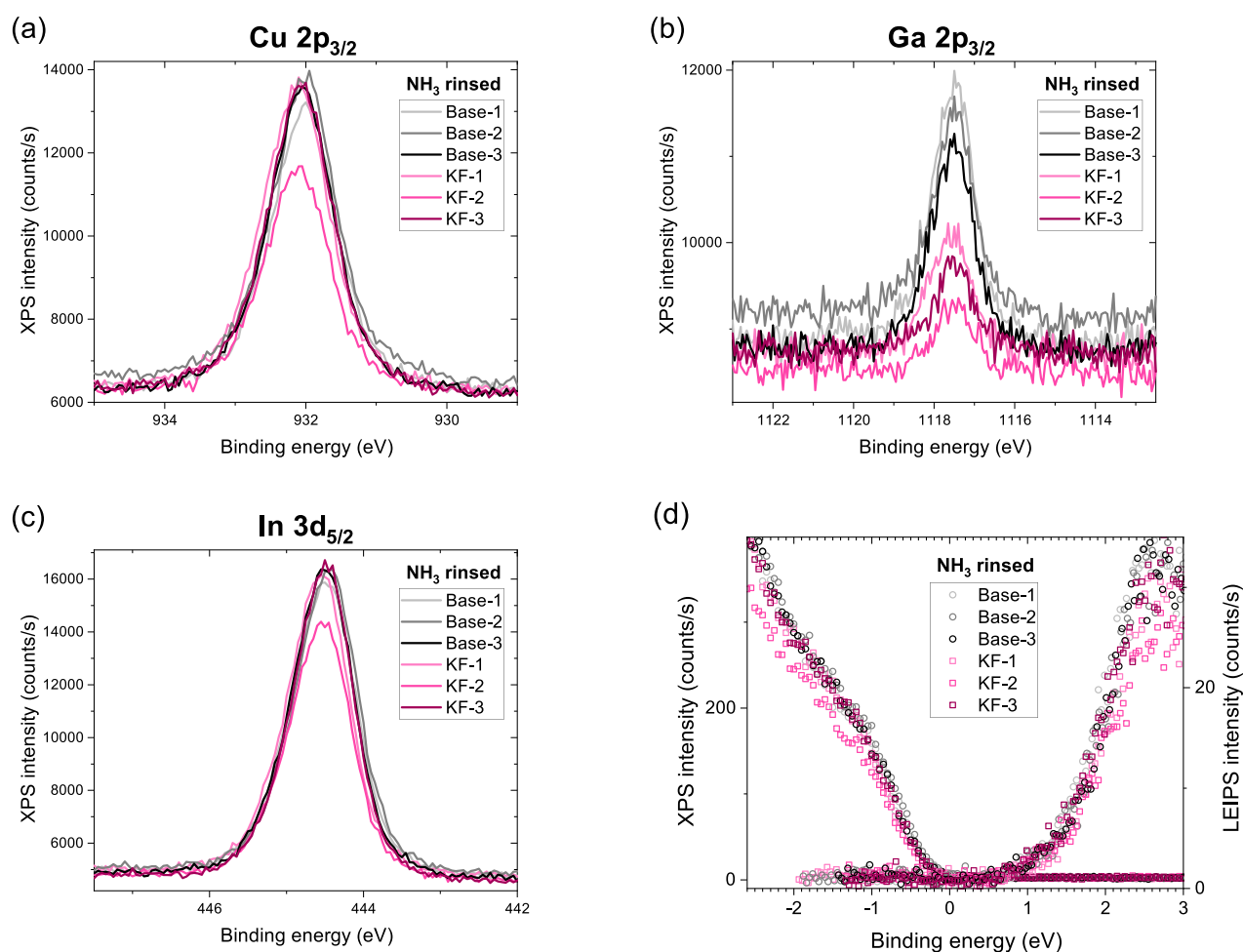In this work, the KF PDT does not increase carrier concentration or Cd in-diffusion, but instead improves

**Figure 3.** XPS detailed spectra of the (a) Cu $2p_{3/2}$, (b) Ga $2p_{3/2}$, (c) In $3d_{5/2}$ peaks, and (d) XPS valence band energy relative to Fermi energy ($E_F - E_{VB}$; left axis) and LEIPS conduction band energy relative to Fermi energy ($E_{CB} - E_F$; right axis) for the NH$_3$ rinsed Base-1 (light gray circles), Base-2 (gray circles), Base-3 (black circles), KF-1 (light pink squares), KF-2 (pink squares), and KF-3 (dark pink squares) samples.

**Table 3. Standard Sensitivity Factor-Based Quantification of XPS K, Cu, Ga, In, and Se Compositions after the NH$_3$ Rinse for All Samples, and the Mean Values for the Baseline and KF PDT Sample Types**[a]

| smple | K (%) | Cu (%) | Ga (%) | In (%) | Se (%) |
|---|---|---|---|---|---|
| Base-1 | 0 | 15.6 | 9.9 | 28.5 | 40.9 |
| Base-2 | 0 | 16.4 | 7.8 | 29.6 | 41.5 |
| Base-3 | 0 | 15.2 | 7.7 | 27.7 | 38.5 |
| KF-1 | 0 | 17.1 | 4.7 | 28.5 | 42.1 |
| KF-2 | 0 | 15.0 | 2.9 | 30.9 | 42.3 |
| KF-3 | 4.6 | 16.8 | 4.2 | 29.5 | 39.7 |
| all base | 0 | 15.7(6) | 8.5(12) | 28.6(9) | 40.3(15) |
| all KF | 1.5(27) | 16.3(12) | 3.9(9) | 29.6(12) | 41.3(15) |

[a]Standard deviations are in parentheses.

**Table 4. Corrected Sensitivity Factor-Based Quantification of XPS K, Cu, Ga, In, and Se Compositions after the NH$_3$ Rinse for All Samples, And the Mean Values for the Baseline and KF PDT Sample Types**[a]

| sample | K (%) | Cu (%) | Ga (%) | In (%) | Se (%) |
|---|---|---|---|---|---|
| Base-1 | 0 | 22.4 | 8.5 | 16.5 | 50 |
| Base-2 | 0 | 24.5 | 6.6 | 18.4 | 50 |
| Base-3 | 0 | 23.7 | 6.8 | 18.2 | 50 |
| KF-1 | 0 | 23.8 | 3.8 | 21.2 | 50 |
| KF-2 | 0 | 20.7 | 2.3 | 22.7 | 50 |
| KF-3 | 0 | 24.9 | 2.7 | 22.3 | 50 |
| all base | 0 | 23.5(11) | 7.3(10) | 17.7(10) | 50 |
| all KF | 0 | 23.1(22) | 2.9(8) | 22.1(8) | 50 |

[a]Standard deviations are in parentheses.

efficiency by reducing the surface valence band and moderately passivating. But how can the KF PDT reduce valence band while not changing Cu/(Ga+In) or K/(K+Cu) composition, and why is a KF PDT necessary when growing the film with lower Cu/(Ga+In) should be an equally effective way to reduce the valence band?

The answer to these questions may stem from a key structural difference: Chalcopyrite CuInSe$_2$ and CuIn$_3$Se$_5$ are both tetragonal and only have {001} cation planes of intermixed Cu and In (Figure 6).[92−94] On the other hand,

K$_2$CuIn$_3$Se$_6$ and KInSe$_2$ are monoclinic layered (or 2D) compounds with planes that only intercept weak K−Se bonds.[63,65,95] Like chalcopyrite CuInSe$_2$, K$_2$CuIn$_3$Se$_6$ has a plane of mixed Cu and In, but unlike chalcopyrite, this plane is clad on both sides by planes of In and weakly bound K, as detailed in Table 5. Thus, the K$_2$CuIn$_3$Se$_6$ unit cell can be thought of as a superlattice of epitaxial CuInSe$_2$/KInSe$_2$.

Both CuInSe$_2$/K$_2$CuIn$_3$Se$_6$ and CuInSe$_2$/KInSe$_2$ form 3D/2D structures that are found in all polycrystalline PV absorbers and are thought to passivate.[17] Therefore, KF PDTs may drive
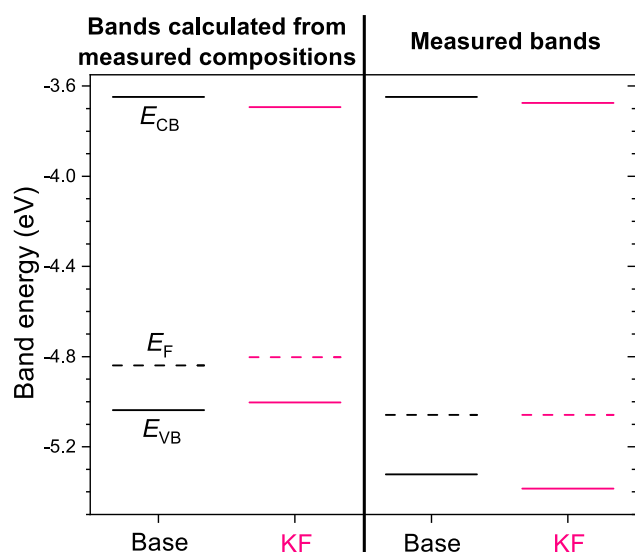
**Figure 4.** Energy relative to vacuum for the base and KF samples' $E_{CB}$, $E_F$, and $E_{VB}$ calculated from the composition data in Table 3, and the same band energy values measured by XPS, LEIPS, and CV (Table 2), respectively, showing that the composition and $E_{VB}$ trends are inconsistent.
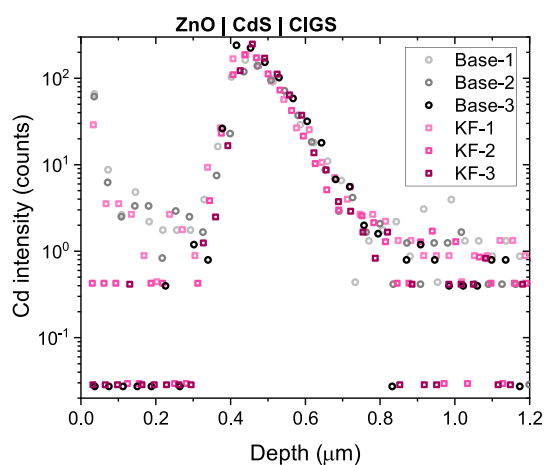


**Figure 5.** SIMS Cd intensity versus depth into the device stack for the Base-1 (light gray circles), Base-2 (gray circles), Base-3 (black circles), KF-1 (light pink squares), KF-2 (pink squares), and KF-3 (dark pink squares).

**Table 5. Se Bond Character by Phase, Site, Cation, Number of Bonds, and Length**

| phase | Se site | bond | no. of bonds | bond length[a] (Å) |
|---|---|---|---|---|
| $CuInSe_2$ | 1 | Se—In | 2 | 2.60[a] |
| | | Se—Cu | 2 | 2.40[b] |
| $KInSe_2$ | 1 | Se—In | 2 | 2.56−2.57 |
| | | Se—K | 4 | 3.41−3.51 |
| | 2 | Se—In | 2 | 2.55−2.56[c] |
| | | Se—K | 2 | 3.26−3.31[d] |
| | | Se—K | 2 | 4.11−4.16[e] |
| $K_2CuIn_3Se_6$ | 1 | Se—In | 2 | 2.57−2.59[a] |
| | | Se—Cu | 1 | 2.45−2.48[b] |
| | | Se—K | 2 | 3.42−3.46 |
| | 2 | Se—In | 2 | 2.56−2.57[c] |
| | | Se—K | 2 | 3.28−3.29[d] |
| | | Se—K | 2 | 4.15[e] |

[a]Similar bonds are noted by superscript letters ([a], [b], [c], [d], and [e]), showing that $K_2CuIn_3Se_6$ can be thought of as a superlattice of epitaxial $CuInSe_2/KInSe_2$.

a reconstructive phase transformation at the surface of chalcopyrite crystals. This topotactic transition reduces the valence band by forming Cu-free planes that are unlike the structure of $CuIn_3Se_5$. Therefore, even if K is mostly rinsed away, it leaves behind a structure that may possess superior passivation despite having identical composition to $CuIn_3Se_5$, for example, $Va_2CuIn_3Se_6$ and $VaInSe_2$ in Figure 6e, f.

Indeed, KF PDTs transform multiple rough 3D grains into smooth, 2D surfaces in scanning spreading resistivity micrographs.[97] The sensitivity of heavy alkali fluoride PDT effectiveness to the presence of $CuIn_3Se_5$ (also known as an ordered defect compound, ordered vacancy compound, or copper deficient layer) is well documented.[44,47,91,98−104] Our proposed mechanism requires that the absorber be Cu-deficient enough to accept the excess Cu generated by forming the Cu-free cation planes at the surface, explaining PDTs' susceptibility to $CuIn_3Se_5$. Alternatively, the formation of Cu-free planes can leave Cu in a soluble form that is rinsed away, explaining why KF PDTs sometimes deplete surface Cu.[1,31−38,40,41,43−51,54−58] Bi is commonly used as a surfactant that reconstructs III−V surfaces to alter ordering during growth.[105] Much like K in CIGS, Bi is isoelectronic but too large to incorporate into III−Vs. These parallels illustrate how KF PDTs are post-growth surfactant treatments used to improve band alignment by reordering surfaces.
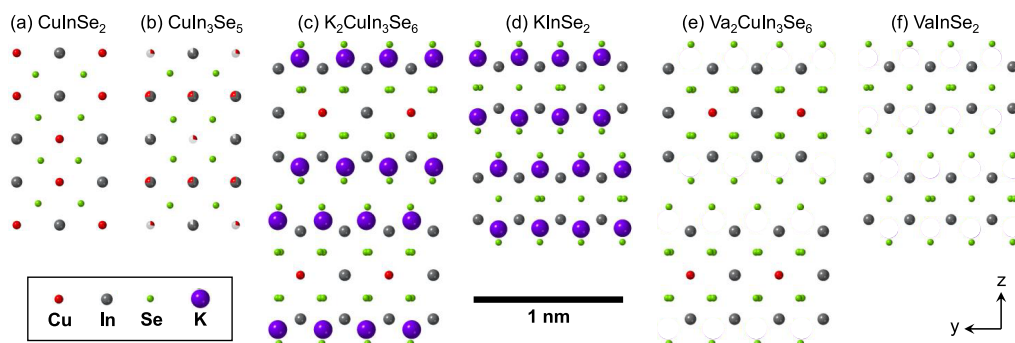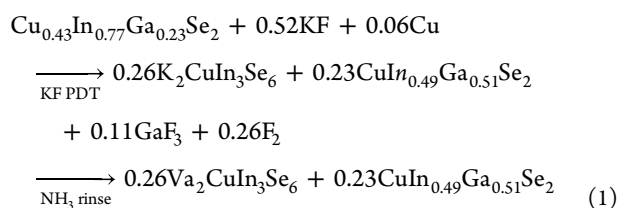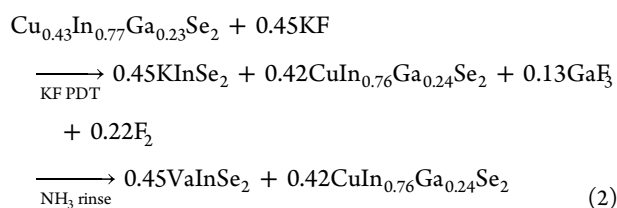


**Figure 6.** Unit cells of the (a) $CuInSe_2$,[96] (b) $CuIn_3Se_5$,[94] (c) $K_2CuIn_3Se_6$,[63] (d) $KInSe_2$,[95] (e) $Va_2CuIn_3Se_6$, and (f) $VaInSe_2$ crystal structures viewed along the [100] direction. Cu is red, In is dark gray, Se is green, and K is purple. Site occupation in $CuIn_3Se_5$ is indicated by pie charts, where vacancies are light gray. $Va_2CuIn_3Se_6$ and $VaInSe_2$ are $K_2CuIn_3Se_6$ and $KInSe_2$ without K.

First-principles calculations generally predict that intragranular K defects in chalcopyrite CIGS are energetically unfavorable or metastable,[21−25] explaining why Na improves KF PDT effectiveness: only through ion exchange[1] is the transfer of K into the lattice energetically favorable.[20] Optimal KF PDT temperatures are ~380 °C, much higher than room temperature and CBD (65 °C) but much lower than absorber growth temperature (550−600 °C). We hypothesize that PDTs require enough thermal energy to break bonds and redistribute atoms in a reconstructive phase transition, while temperature should be low enough to avoid equilibrium.[62,106] Unlike $CuIn_3Se_5$, $CuIn_5Se_8$ does have Cu-free {001} cation planes. As a result, the only first-principles study we are aware of that had structures with Cu-free planes found that $(K−K)_{VaCu}$ dumbbell defects are exceptionally stable in $CuIn_5Se_8$,[107] and we note that such defect structures closely resemble $K_2CuIn_3Se_6$ (Figure 6c).

In order to reconcile the band and composition trends in Figure 4, we propose the following reaction sequence:

$$Cu_{0.43}In_{0.77}Ga_{0.23}Se_2 + 0.52KF + 0.06Cu$$
$$\xrightarrow[\text{KF PDT}]{} 0.26K_2CuIn_3Se_6 + 0.23CuIn_{0.49}Ga_{0.51}Se_2$$
$$+ 0.11GaF_3 + 0.26F_2$$
$$\xrightarrow[\text{NH}_3\text{ rinse}]{} 0.26Va_2CuIn_3Se_6 + 0.23CuIn_{0.49}Ga_{0.51}Se_2 \quad (1)$$

Since the Cu composition increases, Cu is assumed to diffuse from the bulk into the surface during the KF PDT. The $F_2$ evaporates during the PDT while the K and $GaF_3$ are rinsed away. The final products of eq 1 are equivalent to $Cu_{0.49}In_{0.88}Ga_{0.12}Se_2$ but would also match the measured band shifts if $Va_2CuIn_3Se_6$ has an $E_{CB}$ of −0.23 eV and an $E_{VB}$ of −0.38 eV ($E_g$ of +0.15 eV), relative to the initial surface of $Cu_{0.43}In_{0.77}Ga_{0.23}Se_2$ (assuming CIGS bands depend on composition[87] and measured bands are weighted to the products (e.g., $E_{VB,meas}$ = 0.53 $E_{VB,Va2CuIn3Se6}$ + 0.47 $E_{VB,CuIn0.49Ga0.51Se2}$)). If we assume that $KInSe_2$ is formed instead of $K_2CuIn_3Se_6$, then Cu out-diffusion is no longer required:

$$Cu_{0.43}In_{0.77}Ga_{0.23}Se_2 + 0.45KF$$
$$\xrightarrow[\text{KF PDT}]{} 0.45KInSe_2 + 0.42CuIn_{0.76}Ga_{0.24}Se_2 + 0.13GaF_3$$
$$+ 0.22F_2$$
$$\xrightarrow[\text{NH}_3\text{ rinse}]{} 0.45VaInSe_2 + 0.42CuIn_{0.76}Ga_{0.24}Se_2 \quad (2)$$

The final products of eq 2 are equivalent to $Cu_{0.49}In_{0.88}Ga_{0.12}Se_2$ but would also match the measured band shifts if $VaInSe_2$ has an $E_{CB}$ of −0.11 eV and a $E_{VB}$ of −0.41 eV ($E_g$ of +0.30), relative to the initial surface. In conclusion, both eqs 1 and 2 resolve the conflicting band and composition trends if $Va_2CuIn_3Se_6$ and $VaInSe_2$ have similar band structures to $K_2CuIn_3Se_6$,[64] possibly explaining how K can alter bands even after it is gone.

Raman spectroscopy was previously used to distinguish chalcopyrite from "CuAu" cation ordering.[108] KF PDTs have been correlated with a 216 $cm^{−1}$ $E/B_2$ Raman peak and "CuAu" cation ordering.[109] RbF PDTs were also recently correlated with the appearance of a 250 $cm^{−1}$ peak and the disappearance of a 246 $cm^{−1}$ peak, which were attributed to a defective chalcopyrite phase.[99] We propose that these subtle Raman changes could relate to the alkali halide-induced cation reorganization that leads to the Cu-free, weakly bound (2D) planes in Figure 6. Finally, we note that K accumulates at grain surfaces throughout the film (i.e., grain boundaries),[30] so the hypothesized reconstructive band alignment could also improve bulk passivation.

## ■ CONCLUSIONS

KF, RbF, and CsF PDTs have been driving CIGS solar cell performance enhancements for 9 years, but the mechanism remains unclear. Here we characterize KF PDTs by growing multiple samples and performing air-free transfer for XPS. Our KF PDTs do not change majority carrier concentration or Cd in-diffusion, but do increase efficiency by 6.1% absolute, which apparently stems from a moderate recombination reduction (via TRPL) and reduced surface valence band via XPS. However, XPS does not show a significant decrease in Cu/(Ga +In) or increase in K/(K+Cu). We propose that instead, KF PDTs reduce valence band by reconstructing the surface from chalcopyrite CIGS to layered $K_2CuIn_3Se_6$ or $KInSe_2$. The formation of this 3D/2D structure passivates and forms Cu-free cation planes that may reduce valence band even after K is rinsed away.

## ■ AUTHOR INFORMATION

**Corresponding Author**

    **Christopher P. Muzzillo** − *National Renewable Energy Laboratory, Golden, Colorado 80401, United States;* ⊙ orcid.org/0000-0002-6492-0098; Email: christopher.muzzillo@nrel.gov

**Authors**

    **Stephen Glynn** − *National Renewable Energy Laboratory, Golden, Colorado 80401, United States*

    **Glenn Teeter** − *National Renewable Energy Laboratory, Golden, Colorado 80401, United States*

    **Lorelle M. Mansfield** − *National Renewable Energy Laboratory, Golden, Colorado 80401, United States*

Complete contact information is available at:
https://pubs.acs.org/10.1021/acsaem.2c01815

**Notes**

The authors declare no competing financial interest.

## ■ ACKNOWLEDGMENTS

## ■ REFERENCES

(1) Chirilǎ, A.; Reinhard, P.; Pianezzi, F.; Bloesch, P.; Uhl, A. R.; Fella, C.; Kranz, L.; Keller, D.; Gretener, C.; Hagendorfer, H.; Jaeger, D.; Erni, R.; Nishiwaki, S.; Buecheler, S.; Tiwari, A. N. Potassium-induced surface modification of $Cu(In,Ga)Se_2$ thin films for high-efficiency solar cells. *Nat. Mater.* 2013, 12 (12), 1107−1111.

(2) Jackson, P.; Hariskos, D.; Wuerz, R.; Wischmann, W.; Powalla, M. Compositional investigation of potassium doped $Cu(In,Ga)Se_2$ solar cells with efficiencies up to 20.8%. *Phys. Status Solidi RRL* 2014, 8 (3), 219−222.

(3) Kamada, R.; Yagioka, T.; Adachi, S.; Handa, A.; Tai, K. F.; Kato, T.; Sugimoto, H. New world record $Cu(In,Ga)(Se,S)_2$ thin film solar cell efficiency beyond 22%. In *43rd IEEE Photovoltaic Specialists Conference*; Portland, OR, June 5−10, 2016 ; IEEE: Piscataway, NJ, 2016; pp 1287−1291.

(4) Lundberg, O.; Wallin, E.; Gusak, V.; Södergren, S.; Chen, S.; Lotfi, S.; Chalvet, F.; Malm, U.; Kaihovirta, N.; Mende, P.; Jaschke, G.; Kratzert, P.; Joel, J.; Skupinski, M.; Lindberg, P.; Jarmar, T.; Lundberg, J.; Mathiasson, J.; Stolt, L. Improved CIGS Modules by KF Post Deposition Treatment and Reduced Cell-to-Module Losses. In *43rd IEEE Photovoltaic Specialists Conference*; Portland, OR, June 5−10, 2016 ; IEEE: Piscataway, NJ, 2016; pp 1−4.

(5) Jackson, P.; Hariskos, D.; Wuerz, R.; Kiowski, O.; Bauer, A.; Friedlmeier, T. M.; Powalla, M. Properties of $Cu(In,Ga)Se_2$ solar cells with new record efficiencies up to 21.7%. *Phys. Status Solidi RRL* 2015, 9 (1), 28−31.

(6) Jackson, P.; Wuerz, R.; Hariskos, D.; Lotter, E.; Witte, W.; Powalla, M. Effects of heavy alkali elements in $Cu(In,Ga)Se_2$ solar cells with efficiencies up to 22.6%. *Phys. Status Solidi RRL* 2016, 10 (8), 583−586.

(7) Kato, T.; Wu, J.; Hirai, Y.; Sugimoto, H.; Bermudez, V. Record Efficiency for Thin-Film Polycrystalline Solar Cells Up to 22.9% Achieved by Cs-Treated $Cu(In,Ga)(Se,S)_2$. *IEEE J. Photovoltaics* 2019, 9 (1), 325−330.

(8) Nakamura, M.; Yamaguchi, K.; Kimoto, Y.; Yasaki, Y.; Kato, T.; Sugimoto, H. Cd-Free $Cu(In,Ga)(Se,S)_2$ Thin-Film Solar Cell With Record Efficiency of 23.35%. *IEEE J. Photovoltaics* 2019, 9 (6), 1863−1867.

(9) Keyes, B. M.; Hasoon, F.; Dippo, P.; Balcioglu, A.; Abulfotuh, F. Influence of Na on the electro-optical properties of $Cu(In,Ga)Se_2$. In *26th IEEE Photovoltaic Specialists Conference*; Anaheim, CA, Sept 29−Oct 3, 1997 ; IEEE: Piscataway, NJ, 1997; pp 479−482.

(10) Nakada, T.; Iga, D.; Ohbo, H.; Kunioka, A. Effects of Sodium on $Cu(In,Ga)Se_2$-Based Thin Films and Solar Cells. *Jpn. J. Appl. Phys.* 1997, 36 (Part 1, No. 2), 732−737.

(11) Ruckh, M.; Schmid, D.; Kaiser, M.; Schäffler, R.; Walter, T.; Schock, H. W. Influence of substrates on the electrical properties of $Cu(In,Ga)Se_2$ thin films. *Sol. Energy Mater. Sol. Cells* 1996, 41−42, 335−343.

(12) Malitckaya, M.; Komsa, H. P.; Havu, V.; Puska, M. J. Effect of Alkali Metal Atom Doping on the $CuInSe_2$-Based Solar Cell Absorber. *J. Phys. Chem. C* 2017, 121 (29), 15516−15528.

(13) Ishizuka, S.; Taguchi, N.; Fons, P. J. Similarities and Critical Differences in Heavy Alkali-Metal Rubidium and Cesium Effects on Chalcopyrite $Cu(In,Ga)Se_2$ Thin-Film Solar Cells. *J. Phys. Chem. C* 2019, 123 (29), 17757−17764.

(14) Ishizuka, S.; Taguchi, N.; Nishinaga, J.; Kamikawa, Y.; Tanaka, S.; Shibata, H. Group III Elemental Composition Dependence of RbF Postdeposition Treatment Effects on $Cu(In,Ga)Se_2$ Thin Films and Solar Cells. *J. Phys. Chem. C* 2018, 122 (7), 3809−3817.

(15) Lin, T.-Y.; Khatri, I.; Matsuura, J.; Shudo, K.; Huang, W.-C.; Sugiyama, M.; Lai, C.-H.; Nakada, T. Alkali-induced grain boundary reconstruction on $Cu(In,Ga)Se_2$ thin film solar cells using cesium fluoride post deposition treatment. *Nano Energy* 2020, 68, 104299.

(16) Taguchi, N.; Tanaka, S.; Ishizuka, S. Direct insights into $RbInSe_2$ formation at $Cu(In,Ga)Se_2$ thin film surface with RbF postdeposition treatment. *Appl. Phys. Lett.* 2018, 113 (11), 113903.

(17) McGott, D. L.; Muzzillo, C. P.; Perkins, C. L.; Berry, J. J.; Zhu, K.; Duenow, J. N.; Colegrove, E.; Wolden, C. A.; Reese, M. O. 3D/2D passivation as a secret to success for polycrystalline thin-film solar cells. *Joule* 2021, 5 (5), 1057−1073.

(18) Handick, E.; Reinhard, P.; Alsmeier, J.-H.; Köhler, L.; Pianezzi, F.; Krause, S.; Gorgoi, M.; Ikenaga, E.; Koch, N.; Wilks, R. G.; Buecheler, S.; Tiwari, A. N.; Baer, M. Potassium post-deposition treatment-induced band gap widening at $Cu(In,Ga)Se_2$ surfaces - Reason for performance leap? *ACS Appl. Mater. Interfaces* 2015, 7 (49), 27414−27420.

(19) Muzzillo, C. P.; Li, J. V.; Mansfield, L. M.; Ramanathan, K.; Anderson, T. J. Surface and bulk effects of K in highly efficient $Cu_{1-x}K_xInSe_2$ solar cells. *Sol. Energy Mater. Sol. Cells* 2018, 185, 45−53.

(20) Muzzillo, C. P.; Tong, H. M.; Anderson, T. J. The effect of Na on Cu-K-In-Se thin film growth. *J. Cryst. Growth* 2018, 488, 36−42.

(21) Aboulfadl, H.; Sopiha, K. V.; Keller, J.; Larsen, J. K.; Scragg, J. J. S.; Persson, C.; Thuvander, M.; Edoff, M. Alkali Dispersion in $(Ag,Cu)(In,Ga)Se_2$ Thin Film Solar Cells—Insight from Theory and Experiment. *ACS Appl. Mater. Interfaces* 2021, 13 (6), 7188−7199.

(22) Chugh, M.; Kühne, T. D.; Mirhosseini, H. Diffusion of Alkali Metals in Polycrystalline $CuInSe_2$ and Their Role in the Passivation of Grain Boundaries. *ACS Appl. Mater. Interfaces* 2019, 11 (16), 14821−14829.

(23) Kormath Madam Raghupathy, R.; Kühne, T. D.; Henkelman, G.; Mirhosseini, H. Alkali Atoms Diffusion Mechanism in $CuInSe_2$ Explained by Kinetic Monte Carlo Simulations. *Advanced Theory and Simulations* 2019, 2 (6), 1900036.

(24) Sommer, D. E.; Mutter, D.; Dunham, S. T. Defects in Na-, K-, and Cd-Doped $CuInSe_2$: Canonical Thermodynamics Based on Ab Initio Calculations. *IEEE J. Photovoltaics* 2017, 7 (4), 1143−1152.

(25) Yuan, Z.-K.; Chen, S.; Xie, Y.; Park, J.-S.; Xiang, H.; Gong, X.-G.; Wei, S.-H. Na-Diffusion Enhanced p-type Conductivity in $Cu(In,Ga)Se_2$: A New Mechanism for Efficient Doping in Semiconductors. *Adv. Energy Mater.* 2016, 6 (24), 1601191.

(26) Muzzillo, C. P.; Poplawsky, J. D.; Tong, H. M.; Guo, W.; Anderson, T. Revealing the beneficial role of K in grain interiors, grain boundaries, and at the buffer interface for highly efficient $CuInSe_2$ solar cells. *Progress in Photovoltaics: Research and Applications* 2018, 26 (10), 825−834.

(27) Lanzoni, E. M.; Ramírez, O.; Phirke, H.; Elizabeth, A.; Mönig, H.; Redinger, A. Impact of metallic potassium post-deposition treatment on epitaxial $Cu(In,Ga)Se_2$. *Thin Solid Films* 2022, 741, 139002.

(28) Ramírez, O.; Bertrand, M.; Debot, A.; Siopa, D.; Valle, N.; Schmauch, J.; Melchiorre, M.; Siebentritt, S. The Effect of Potassium Fluoride Postdeposition Treatments on the Optoelectronic Properties of $Cu(In,Ga)Se_2$ Single Crystals. *Solar RRL* 2021, 5 (4), 2000727.

(29) Wuerz, R.; Hempel, W.; Jackson, P. Diffusion of Rb in polycrystalline $Cu(In,Ga)Se_2$ layers and effect of Rb on solar cell parameters of $Cu(In,Ga)Se_2$ thin-film solar cells. *J. Appl. Phys.* 2018, 124 (16), 165305.

(30) Muzzillo, C. P. Review of grain interior, grain boundary, and interface effects of K in CIGS solar cells: Mechanisms for performance enhancement. *Sol. Energy Mater. Sol. Cells* 2017, 172 (Supplement C), 18−24.

(31) Donzel-Gargand, O.; Larsson, F.; Törndahl, T.; Stolt, L.; Edoff, M. Secondary phase formation and surface modification from a high dose KF-post deposition treatment of $(Ag,Cu)(In,Ga)Se_2$ solar cell absorbers. *Progress in Photovoltaics: Research and Applications* 2019, 27 (3), 220−228.

(32) Khatri, I.; Fukai, H.; Yamaguchi, H.; Sugiyama, M.; Nakada, T. Effect of potassium fluoride post-deposition treatment on $Cu(In,Ga)-Se_2$ thin films and solar cells fabricated onto sodalime glass substrates. *Sol. Energy Mater. Sol. Cells* 2016, 155, 280−287.

(33) Khatri, I.; Shudo, K.; Matsuura, J.; Sugiyama, M.; Nakada, T. Comparative study of water and ammonia rinsing processes of potassium fluoride-treated $Cu(In,Ga)Se_2$ thin film solar cells. *Jpn. J. Appl. Phys.* 2017, 56 (8S2), 08MC12.

(34) Khatri, I.; Sugiyama, M.; Nakada, T. Effects of combined additional indium deposition and potassium fluoride post-deposition

treatments on $Cu(In,Ga)Se_2$ thin film solar cells. *Progress in Photovoltaics: Research and Applications* **2017**, *25*, 871−877.

(35) Lee, W.-J.; Cho, D.-H.; Wi, J.-H.; Yu, J. H.; Kim, W.-J.; Kang, C.; Kang, S. J.; Chung, Y.-D. Evolution of Morphological and Chemical Properties at p-n Junction of $Cu(In,Ga)Se_2$ Solar Cells with $Zn(O,S)$ Buffer Layer as a Function of KF Postdeposition Treatment Time. *ACS Appl. Mater. Interfaces* **2021**, *13* (41), 48611−48621.

(36) Shin, D.; Kim, J.; Gershon, T.; Mankad, R.; Hopstaken, M.; Guha, S.; Ahn, B. T.; Shin, B. Effects of the incorporation of alkali elements on $Cu(In,Ga)Se_2$ thin film solar cells. *Sol. Energy Mater. Sol. Cells* **2016**, *157*, 695−702.

(37) Yang, P.; Wilks, R. G.; Yang, W.; Bär, M. Interface Formation between CdS and Alkali Postdeposition-Treated $Cu(In,Ga)Se_2$ Thin-Film Solar Cell Absorbers—Key To Understanding the Efficiency Gain. *ACS Appl. Mater. Interfaces* **2020**, *12* (5), 6688−6698.

(38) Zheng, X.; Xie, C.; Li, W.; Aberle, A. G.; Venkataraj, S. Investigations of potassium-induced surface treatment of $Cu(In,Ga)-Se_2$ (CIGSe) thin film solar cells prepared by two-stage process using elemental selenium. *Appl. Surf. Sci.* **2020**, *525*, 146368.

(39) Hsu, C.-H.; Ho, W.-H.; Wei, S.-Y.; Lai, C.-H. Over 14% Efficiency of Directly Sputtered $Cu(In,Ga)Se_2$ Absorbers without Postselenization by Post-Treatment of Alkali Metals. *Adv. Energy Mater.* **2017**, *7* (13), 1602571.

(40) Cai, C.-H.; Chen, R.-Z.; Chan, T.-S.; Lu, Y.-R.; Huang, W.-C.; Yen, C.-C.; Zhao, K.; Lo, Y.-C.; Lai, C.-H. Interplay between potassium doping and bandgap profiling in selenized $Cu(In,Ga)Se_2$ solar cells: A functional CuGa:KF surface precursor layer. *Nano Energy* **2018**, *47*, 393−400.

(41) Zhao, Y.-H.; Gao, Q.-Q.; Yuan, S.-J.; Chang, Q.-Q.; Liang, T.; Su, Z.-H.; Ma, H.-L.; Chen, S.; Liang, G.-X.; Fan, P.; Zhang, X.-H.; Wu, S.-X. Defects Passivation and Crystal Growth Promotion by Solution-Processed K Doping Strategy toward 16.02% Efficiency $Cu(In,Ga)(S,Se)_2$ Solar Cells. *Chem. Eng. J.* **2022**, *436*, 135008.

(42) Chen, J.; Shen, H.; Zhai, Z.; Liu, F.; Zhu, Z.; Luo, M. Performance and stability enhancement of $Cu(InGa)Se_2$ solar cells on ultrathin glass by potassium incorporation. *Mater. Lett.* **2020**, *271*, 127749.

(43) Alruqobah, E. H.; Agrawal, R. Potassium Treatments for Solution-Processed $Cu(In,Ga)(S,Se)_2$ Solar Cells. *ACS Applied Energy Materials* **2020**, *3* (5), 4821−4830.

(44) Balestrieri, M.; Achard, V.; Hildebrandt, T.; Lombez, L.; Jubault, M.; Béchu, S.; Bouttemy, M.; Etcheberry, A.; Lincot, D.; Donsanti, F. Improving $V_{oc}$ With Indium and Alkali Fluorides in $Cu(In,Ga)Se_2$ Solar Cells Deposited at Low Temperature on Polyimide. *IEEE J. Photovoltaics* **2018**, *8* (5), 1343−1348.

(45) Handick, E.; Reinhard, P.; Wilks, R. G.; Pianezzi, F.; Félix, R.; Gorgoi, M.; Kunze, T.; Buecheler, S.; Tiwari, A. N.; Bär, M. NaF/KF Post-Deposition Treatments and their Influence on the Structure of $Cu(In,Ga)Se_2$ Absorber Surfaces. In *43rd IEEE Photovoltaic Specialists Conference*; Portland, OR, June 5−10, 2016 ; IEEE: Piscataway, NJ, 2016; pp 1−5.

(46) Handick, E.; Reinhard, P.; Wilks, R. G.; Pianezzi, F.; Kunze, T.; Kreikemeyer-Lorenzo, D.; Weinhardt, L.; Blum, M.; Yang, W.; Gorgoi, M.; Ikenaga, E.; Gerlach, D.; Ueda, S.; Yamashita, Y.; Chikyow, T.; Heske, C.; Buecheler, S.; Tiwari, A. N.; Bär, M. Formation of a K-In-Se surface species by NaF/KF post-deposition treatment of $Cu(In,Ga)Se_2$ thin-film solar cell absorbers. *ACS Appl. Mater. Interfaces* **2017**, *9* (4), 3581−3589.

(47) Lepetit, T.; Harel, S.; Arzel, L.; Ouvrard, G.; Barreau, N. KF post deposition treatment in co-evaporated $Cu(In,Ga)Se_2$ thin film solar cells: Beneficial or detrimental effect induced by the absorber characteristics. *Progress in Photovoltaics: Research and Applications* **2017**, *25* (12), 1068−1076.

(48) Majumdar, I.; Ümsür, B.; Chacko, B.; Greiner, D.; Lux-Steiner, M. C.; Schlatmann, R.; Lauermann, I. Surface Modifications of Na and K Metal Incorporated $Cu(In,Ga)Se_2$ Absorbers Investigated by Synchrotron-Based Spectroscopies. *physica status solidi c* **2017**, *14* (10), 1700167.

(49) Mezher, M.; Mansfield, L. M.; Horsley, K.; Yang, W.; Blum, M.; Weinhardt, L.; Ramanathan, K.; Heske, C. Variations in the Chemical and Electronic Impact of Post-Deposition Treatments on $Cu(In,Ga)-(S,Se)_2$ Absorbers. *ACS Applied Energy Materials* **2019**, *2* (12), 8641−8648.

(50) Pistor, P.; Greiner, D.; Kaufmann, C. A.; Brunken, S.; Gorgoi, M.; Steigert, A.; Calvet, W.; Lauermann, I.; Klenk, R.; Unold, T.; Lux-Steiner, M.-C. Experimental indication for band gap widening of chalcopyrite solar cell absorbers after potassium fluoride treatment. *Appl. Phys. Lett.* **2014**, *105* (6), 063901−063904.

(51) Nagai, T.; Nishinaga, J.; Tampo, H.; Kim, S.; Hirayama, K.; Matsunobe, T.; Chen, G.; Ide, Y.; Ishizuka, S.; Shibata, H.; Niki, S.; Terada, N. Impacts of KF Post-Deposition Treatment on the Band Alignment of Epitaxial $Cu(In,Ga)Se_2$ Heterojunctions. *ACS Appl. Mater. Interfaces* **2022**, *14* (14), 16780−16790.

(52) Mansfield, L. M.; Noufi, R.; Muzzillo, C. P.; DeHart, C.; Bowers, K.; To, B.; Pankow, J. W.; Reedy, R. C.; Ramanathan, K. Enhanced performance in $Cu(In,Ga)Se_2$ solar cells fabricated by the two-step selenization process with a potassium fluoride postdeposition treatment. *IEEE J. Photovoltaics* **2014**, *4* (6), 1650−1654.

(53) Larsson, F.; Donzel-Gargand, O.; Keller, J.; Edoff, M.; Törndahl, T. Atomic layer deposition of $Zn(O,S)$ buffer layers for $Cu(In,Ga)Se_2$ solar cells with KF post-deposition treatment. *Sol. Energy Mater. Sol. Cells* **2018**, *183*, 8−15.

(54) Kato, T.; Handa, A.; Yagioka, T.; Matsuura, T.; Yamamoto, K.; Higashi, S.; Wu, J.-L.; Tai, K. F.; Hiroi, H.; Yoshiyama, T.; Sakai, T.; Sugimoto, H. Enhanced efficiency of Cd-free $Cu(In,Ga)(Se,S)_2$ minimodule via $(Zn,Mg)O$ second buffer layer and alkali metal post-treatment. *IEEE J. Photovoltaics* **2017**, *7* (6), 1773−1780.

(55) Valdes, N. H.; Jones, K. J.; Opila, R. L.; Shafarman, W. N. Influence of Ga and Ag on the KF Treatment Chemistry for CIGS Solar Cells. *IEEE J. Photovoltaics* **2019**, *9* (6), 1846−1851.

(56) Lee, J. H.; Tsvetkov, N.; Kim, S. T.; Kim, K.; Yun, J. H.; Larina, L.; Ahn, B. T. Surface modification of $Cu(In,Ga)Se_2$ film with a post deposition treatment using a KI solution and its effect on solar cell performance. *Solar RRL* **2022**, *6*, 2200058.

(57) Reinhard, P.; Bissig, B.; Pianezzi, F.; Avancini, E.; Hagendorfer, H.; Keller, D.; Fuchs, P.; Döbeli, M.; Vigo, C.; Crivelli, P.; Nishiwaki, S.; Buecheler, S.; Tiwari, A. N. Features of KF and NaF Postdeposition Treatments of $Cu(In,Ga)Se_2$ Absorbers for High Efficiency Thin Film Solar Cells. *Chem. Mater.* **2015**, *27* (16), 5755−5764.

(58) Umsur, B.; Calvet, W.; Steigert, A.; Lauermann, I.; Gorgoi, M.; Prietzel, K.; Greiner, D.; Kaufmann, C. A.; Unold, T.; Lux-Steiner, M. Investigation of the potassium fluoride post deposition treatment on the CIGSe/CdS interface using hard x-ray photoemission spectroscopy - a comparative study. *Phys. Chem. Chem. Phys.* **2016**, *18* (20), 14129−14138.

(59) Mezher, M.; Mansfield, L. M.; Horsley, K.; Blum, M.; Wieting, R.; Weinhardt, L.; Ramanathan, K.; Heske, C. KF post-deposition treatment of industrial $Cu(In, Ga)(S, Se)_2$ thin-film surfaces: Modifying the chemical and electronic structure. *Appl. Phys. Lett.* **2017**, *111* (7), 071601.

(60) Rusu, M.; Kodalle, T.; Choubrac, L.; Barreau, N.; Kaufmann, C. A.; Schlatmann, R.; Unold, T. Electronic Structure of the CdS/$Cu(In,Ga)Se_2$ Interface of KF- and RbF-Treated Samples by Kelvin Probe and Photoelectron Yield Spectroscopy. *ACS Appl. Mater. Interfaces* **2021**, *13* (6), 7745−7755.

(61) Kish, Z. Z.; Lazarev, V. B.; Peresh, E. Y.; Semrad, E. E. Compounds in $In_2Se_3$-$K_2Se$. *Neorg. Mater.* **1988**, *24* (10), 1602−1605.

(62) Muzzillo, C. P.; Tong, H. M.; Anderson, T. J. Chemistry of K in $Cu(In,Ga)Se_2$ photovoltaic absorbers: effects of temperature on Cu-K-In-Se films. *J. Alloys Compd.* **2017**, *726*, 538−546.

(63) Ma, H.-W.; Guo, G.-C.; Wang, M.-S.; Zhou, G.-W.; Lin, S.-H.; Dong, Z.-C.; Huang, J.-S. $K_2MM'_3Se_6$ (M = Cu, Ag; M' = Ga, In), A New Series of Metal Chalcogenides with Chain-Sublayer-Chain Slabs: $_\infty^1[M'Se_4]$-$_\infty^2[(MSe_4)(M'Se_4)]$-$_\infty^1[M'Se_4]$. *Inorg. Chem.* **2003**, *42* (4), 1366−1370.

(64) Muzzillo, C. P.; Mansfield, L. M.; Ramanathan, K.; Anderson, T. J. Properties of $Cu_{1-x}K_xInSe_2$ alloys. *J. Mater. Sci.* **2016**, *51* (14), 6812−6823.

(65) Wang, G.-H.; Guo, H.-Y. Solid-state synthesis of $K_2CuIn_3Se_6$ and its crystal structure and characterization. *Journal of Beijing University of Chemical Technology* **2004**, *31* (2), 73−77.

(66) Muzzillo, C. P.; Anderson, T. J. Surface and bulk effects of K in $Cu_{1-x}K_xIn_{1-y}Ga_ySe_2$ solar cells. *Sol. Energy Mater. Sol. Cells* **2018**, *179*, 362−371.

(67) Jeong, G. S.; Cha, E. S.; Moon, S. H.; Ahn, B. T. Effect of KF Treatment of $Cu(In,Ga)Se_2$ Thin Films on the Photovoltaic Properties of CIGS Solar Cells. *Curr. Photovoltaic Res.* **2015**, *3* (2), 65−70.

(68) Siebentritt, S.; Avancini, E.; Bär, M.; Bombsch, J.; Bourgeois, E.; Buecheler, S.; Carron, R.; Castro, C.; Duguay, S.; Félix, R.; Handick, E.; Hariskos, D.; Havu, V.; Jackson, P.; Komsa, H.-P.; Kunze, T.; Malitckaya, M.; Menozzi, R.; Nesladek, M.; Nicoara, N.; Puska, M.; Raghuwanshi, M.; Pareige, P.; Sadewasser, S.; Sozzi, G.; Tiwari, A. N.; Ueda, S.; Vilalta-Clemente, A.; Weiss, T. P.; Werner, F.; Wilks, R. G.; Witte, W.; Wolter, M. H. Heavy Alkali Treatment of $Cu(In,Ga)Se_2$ Solar Cells: Surface versus Bulk Effects. *Adv. Energy Mater.* **2020**, *10* (8), 1903752.

(69) Eslam, A.; Wuerz, R.; Hauschild, D.; Weinhardt, L.; Hempel, W.; Powalla, M.; Heske, C. Impact of substrate temperature during NaF and KF post-deposition treatments on chemical and optoelectronic properties of alkali-free $Cu(In,Ga)Se_2$ thin film solar cell absorbers. *Thin Solid Films* **2021**, *739*, 138979.

(70) Hauschild, D.; Kreikemeyer-Lorenzo, D.; Jackson, P.; Friedlmeier, T. M.; Hariskos, D.; Reinert, F.; Powalla, M.; Heske, C.; Weinhardt, L. Impact of a RbF postdeposition treatment on the electronic structure of the $CdS/Cu(In,Ga)Se_2$ heterojunction in high-efficiency thin-film solar cells. *ACS Energy Letters* **2017**, *2* (10), 2383−2387.

(71) Bombsch, J.; Avancini, E.; Carron, R.; Handick, E.; Garcia-Diez, R.; Hartmann, C.; Félix, R.; Ueda, S.; Wilks, R. G.; Bär, M. NaF/RbF-Treated $Cu(In,Ga)Se_2$ Thin-Film Solar Cell Absorbers: Distinct Surface Modifications Caused by Two Different Types of Rubidium Chemistry. *ACS Appl. Mater. Interfaces* **2020**, *12* (31), 34941−34948.

(72) Cheng, S.; Zhang, K.; Lin, S.; Zhang, Y.; Sun, Y.; Liu, W. Analysis of the Heavy Alkali Element Postdeposition Treatment: Which Factors Determine the Electronic Structure and Transport Properties of the Heterojunction in CIGS Thin Film Solar Cells. *ACS Applied Energy Materials* **2021**, *4* (4), 3279−3287.

(73) Cheng, S.; Zhang, K.; Zhang, Y.; He, Z.; Liang, B.; Du, Q.; Sun, Y.; Liu, W. Effects of different Cs distribution in the film on the performance of CIGS thin film solar cells. *Sol. Energy Mater. Sol. Cells* **2021**, *222*, 110917.

(74) Avancini, E.; Carron, R.; Weiss, T. P.; Andres, C.; Bürki, M.; Schreiner, C.; Figi, R.; Romanyuk, Y. E.; Buecheler, S.; Tiwari, A. N. Effects of Rubidium Fluoride and Potassium Fluoride Postdeposition Treatments on $Cu(In,Ga)Se_2$ Thin Films and Solar Cell Performance. *Chem. Mater.* **2017**, *29* (22), 9695−9704.

(75) Kodalle, T.; Heinemann, M. D.; Greiner, D.; Yetkin, H. A.; Klupsch, M.; Li, C.; van Aken, P. A.; Lauermann, I.; Schlatmann, R.; Kaufmann, C. A. Elucidating the Mechanism of an RbF Post Deposition Treatment in CIGS Thin Film Solar Cells. *Solar RRL* **2018**, *2* (9), 1800156.

(76) Kreikemeyer-Lorenzo, D.; Hauschild, D.; Jackson, P.; Friedlmeier, T. M.; Hariskos, D.; Blum, M.; Yang, W.; Reinert, F.; Powalla, M.; Heske, C.; Weinhardt, L. Rubidium Fluoride Post-Deposition Treatment: Impact on the Chemical Structure of the $Cu(In,Ga)Se_2$ Surface and $CdS/Cu(In,Ga)Se_2$ Interface in Thin-Film Solar Cells. *ACS Appl. Mater. Interfaces* **2018**, *10* (43), 37602−37608.

(77) Majumdar, I.; Sahoo, S. K.; Parvan, V.; Mirhosseini, H.; Chacko, B.; Wang, Y.; Greiner, D.; Kühne, T. D.; Schlatmann, R.; Lauermann, I. Effects of KF and RbF treatments on $Cu(In,Ga)Se_2$-based solar cells: A combined photoelectron spectroscopy and DFT study. *Appl. Surf. Sci.* **2021**, *538*, 148085.

(78) Martin, N. M.; Törndahl, T.; Wallin, E.; Simonov, K. A.; Rensmo, H.; Platzer-Björkman, C. Surface/Interface Effects by Alkali Postdeposition Treatments of $(Ag,Cu)(In,Ga)Se_2$ Thin Film Solar Cells. *ACS Applied Energy Materials* **2022**, *5*, 461−468.

(79) Maticiuc, N.; Kodalle, T.; Lauche, J.; Wenisch, R.; Bertram, T.; Kaufmann, C. A.; Lauermann, I. In vacuo XPS investigation of $Cu(In,Ga)Se_2$ surface after RbF post-deposition treatment. *Thin Solid Films* **2018**, *665*, 143−147.

(80) Maticiuc, N.; Kodalle, T.; Ümsür, B.; Bertram, T.; Wenisch, R.; Wang, Y.; Majumdar, I.; Yetkin, H. A.; Abou-Ras, D.; Schäfer, N.; Kaufmann, C. A.; Schlatmann, R.; Lauermann, I. Depth-resolved analysis of the effect of RbF post deposition treatment on CIGSe with two different Cu concentrations. *Sol. Energy Mater. Sol. Cells* **2021**, *226*, 111071.

(81) Ümsür, B.; Maticiuc, N.; Kodalle, T.; Wenisch, R.; Majumdar, I.; Wang, Y.; Yetkin, H. A.; Bertram, T.; Kaufmann, C. A.; Schlatmann, R.; Lauermann, I. Impact of RbF post deposition treatment on $CdS/CIGSe$ and $Zn(O,S)/CIGSe$ interfaces - A comparative HAXPES study. *Renewable Energy* **2021**, *180*, 626−636.

(82) Keller, J.; Aboulfadl, H.; Stolt, L.; Donzel-Gargand, O.; Edoff, M. Rubidium fluoride absorber treatment for wide-gap $(Ag,Cu)$-$(In,Ga)Se_2$ solar cells. *Solar RRL* **2022**, *6*, 2200044.

(83) Beppu, K.; Hirai, Y.; Kato, T.; Ishizuka, S.; Ina, T.; Wada, T. Effect of cesium for $Cu(In,Ga)Se_2$ and $Cu(In,Ga)(S,Se)_2$ films studied by depth-resolved XAFS. *Appl. Phys. Lett.* **2020**, *117* (4), 043901.

(84) Liu, Y.; Sun, Y.; Rockett, A. A new simulation software of solar cells—wxAMPS. *Sol. Energy Mater. Sol. Cells* **2012**, *98*, 124−128.

(85) Zhu, H.; Kalkan, A. K.; Hou, J.; Fonash, S. J. Applications of AMPS-1D for solar cell simulation. *AIP Conf. Proc.* **1999**, *462* (1), 309−314.

(86) Witte, W.; Abou-Ras, D.; Albe, K.; Bauer, G. H.; Bertram, F.; Boit, C.; Brüggemann, R.; Christen, J.; Dietrich, J.; Eicke, A.; Hariskos, D.; Maiberg, M.; Mainz, R.; Meessen, M.; Müller, M.; Neumann, O.; Orgis, T.; Paetel, S.; Pohl, J.; Rodriguez-Alvarez, H.; Scheer, R.; Schock, H.-W.; Unold, T.; Weber, A.; Powalla, M. Gallium gradients in $Cu(In,Ga)Se_2$ thin-film solar cells. *Progress in Photovoltaics: Research and Applications* **2015**, *23* (6), 717−733.

(87) Stokes, A.; Al-Jassim, M.; Norman, A.; Diercks, D.; Gorman, B. Nanoscale insight into the p−n junction of alkali-incorporated $Cu(In,Ga)Se_2$ solar cells. *Progress in Photovoltaics: Research and Applications* **2017**, *25* (9), 764−772.

(88) Friedlmeier, T. M.; Jackson, P.; Kreikemeyer-Lorenzo, D.; Hauschild, D.; Kiowski, O.; Hariskos, D.; Weinhardt, L.; Heske, C.; Powalla, M. A Closer Look at Initial CdS Growth on High-Efficiency $Cu(In,Ga)Se_2$ Absorbers Using Surface-Sensitive Methods. In *43rd IEEE Photovoltaic Specialists Conference*; Portland, OR, June 5−10, 2016 ; IEEE: Piscataway, NJ, 2016; pp 1−5.

(89) Li, H.; Malliakas, C. D.; Peters, J. A.; Liu, Z.; Im, J.; Jin, H.; Morris, C. D.; Zhao, L.-D.; Wessels, B. W.; Freeman, A. J.; Kanatzidis, M. G. $CsCdInQ_3$ (Q = Se, Te): New Photoconductive Compounds As Potential Materials for Hard Radiation Detection. *Chem. Mater.* **2013**, *25* (10), 2089−2099.

(90) Lepetit, T.; Harel, S.; Arzel, L.; Ouvrard, G.; Barreau, N. Coevaporated $KInSe_2$: A Fast Alternative to KF Postdeposition Treatment in High-Efficiency $Cu(In,Ga)Se_2$ Thin Film Solar Cells. *IEEE J. Photovoltaics* **2016**, *6* (5), 1316−1320.

(91) Harel, S.; Arzel, L.; Lepetit, T.; Zabierowski, P.; Barreau, N. Influence of Sulfur Evaporation during or after KF-Post Deposition Treatment On $Cu(In,Ga)Se_2/CdS$ Interface Formation. *ACS Appl. Mater. Interfaces* **2020**, *12* (41), 46953−46962.

(92) Lehmann, S.; Marrón, D. F.; León, M.; Feyerherm, R.; Dudzik, E.; Friedrich, E. J.; Tovar, M.; Tomm, Y.; Wolf, C.; Schorr, S.; et al. Long-range structure of $Cu(In_xGa_{1-x})_3Se_5$: A complementary neutron and anomalous x-ray diffraction study. *J. Appl. Phys.* **2011**, *109* (1), 013518−013511.

(93) Maeda, T.; Gong, W.; Wada, T. Crystallographic and optical properties and band structures of $CuInSe_2$, $CuIn_3Se_5$, and $CuIn_5Se_8$

phases in Cu-poor $Cu_2Se$-$In_2Se_3$ pseudo-binary system. *Jpn. J. Appl. Phys.* **2016**, *55* (4S), 04ES15.

(94) Paszkowicz, W.; Lewandowska, R.; Bacewicz, R. Rietveld refinement for $CuInSe_2$ and $CuIn_3Se_5$. *J. Alloys Compd.* **2004**, *362* (1), 241−247.

(95) Wang, P.; Huang, X.-Y.; Liu, Y.-L.; Wei, Y.-G.; Li, J.; Guo, H.-Y. Solid state synthesis at intermediate temperature and structural characterization of $KInSe_2$. *Acta Chim. Sinica* **2000**, *58* (8), 1005−1008.

(96) Hahn, H.; Frank, G.; Klingler, W.; Meyer, A.-D.; Störger, G. Untersuchungen über ternäre Chalkogenide. V. Über einige ternäre Chalkogenide mit Chalkopyritstruktur. *Zeitschrift für anorganische und allgemeine Chemie* **1953**, *271* (3−4), 153−170.

(97) Jiang, C. S.; To, B.; Glynn, S.; Mahabaduge, H.; Barnes, T.; Al-Jassim, M. M. Recent progress in nanoelectrical characterizations of CdTe and $Cu(In, Ga)Se_2$. In *2016 IEEE 43rd Photovoltaic Specialists Conference (PVSC)*; Portland, OR, June 5−10, 2016 ; IEEE: Piscataway, NJ, 2016; pp 3675−3680.

(98) Donzel-Gargand, O.; Thersleff, T.; Keller, J.; Törndahl, T.; Larsson, F.; Wallin, E.; Stolt, L.; Edoff, M. Deep surface Cu depletion induced by K in high-efficiency $Cu(In,Ga)Se_2$ solar cell absorbers. *Progress in Photovoltaics: Research and Applications* **2018**, *26* (9), 730−739.

(99) Fonoll-Rubio, R.; Paetel, S.; Grau-Luque, E.; Becerril-Romero, I.; Mayer, R.; Pérez-Rodríguez, A.; Guc, M.; Izquierdo-Roca, V. Insights into the Effects of RbF-Post-Deposition Treatments on the Absorber Surface of High Efficiency $Cu(In,Ga)Se_2$ Solar Cells and Development of Analytical and Machine Learning Process Monitoring Methodologies Based on Combinatorial Analysis. *Adv. Energy Mater.* **2022**, *12*, 2103163.

(100) Ishizuka, S.; Fons, P. J. Role of the Cu-Deficient Interface in $Cu(In,Ga)Se_2$ Thin-Film Photovoltaics with Alkali-Metal Doping. *Physical Review Applied* **2021**, *15* (5), 054005.

(101) Kodalle, T.; Bertram, T.; Schlatmann, R.; Kaufmann, C. A. Effectiveness of an RbF post deposition treatment of CIGS solar cells in dependence on the Cu content of the absorber layer. *IEEE J. Photovoltaics* **2019**, *9*, 1−7.

(102) Kodalle, T.; Choubrac, L.; Arzel, L.; Schlatmann, R.; Barreau, N.; Kaufmann, C. A. Effects of KF and RbF post deposition treatments on the growth of the CdS buffer layer on CIGS thin films - a comparative study. *Sol. Energy Mater. Sol. Cells* **2019**, *200*, 109997.

(103) Sadono, A.; Hino, M.; Nakada, K.; Yamada, A. Effect of an additional Cu-deficient layer deposition on alkali treated $Cu(In,Ga)$-$Se_2$ solar cells deposited at low temperature. *Sol. Energy Mater. Sol. Cells* **2018**, *184*, 67−72.

(104) Tsoulka, P.; Crossay, A.; Arzel, L.; Harel, S.; Barreau, N. Alternative alkali fluoride post-deposition treatment under elemental sulfur atmosphere for high-efficiency $Cu(In,Ga)Se_2$-based solar cells. *Progress in Photovoltaics: Research and Applications* **2021**, *30*, 835.

(105) Jun, S. W.; Fetzer, C. M.; Lee, R. T.; Shurtleff, J. K.; Stringfellow, G. B. Bi surfactant effects on ordering in GaInP grown by organometallic vapor-phase epitaxy. *Appl. Phys. Lett.* **2000**, *76* (19), 2716−2718.

(106) Holder, A. M.; Siol, S.; Ndione, P. F.; Peng, H.; Deml, A. M.; Matthews, B. E.; Schelhas, L. T.; Toney, M. F.; Gordon, R. G.; Tumas, W.; Perkins, J. D.; Ginley, D. S.; Gorman, B. P.; Tate, J.; Zakutayev, A.; Lany, S. Novel phase diagram behavior and materials design in heterostructural semiconductor alloys. *Science Advances* **2017**, *3* (6), No. e1700270.

(107) Ghorbani, E.; Kiss, J.; Mirhosseini, H.; Roma, G.; Schmidt, M.; Windeln, J.; Kühne, T. D.; Felser, C. Hybrid-Functional Calculations on the Incorporation of Na and K Impurities into the $CuInSe_2$ and $CuIn_5Se_8$ Solar-Cell Materials. *J. Phys. Chem. C* **2015**, *119* (45), 25197−25203.

(108) Stanbery, B. J.; Kincal, S.; Kim, S.; Chang, C. H.; Ahrenkiel, S. P.; Lippold, G.; Neumann, H.; Anderson, T. J.; Crisalle, O. D. Epitaxial growth and characterization of $CuInSe_2$ crystallographic polytypes. *J. Appl. Phys.* **2002**, *91* (6), 3598−3604.

(109) Nietzold, T.; Valdes, N.; Stuckelberger, M. E.; Chiu, M.; Walker, T.; Jeffries, A. M.; Sinha, A.; Schelhas, L. T.; Lai, B.; Shafarman, W. N.; Bertoni, M. I. Role of Cation Ordering on Device Performance in $(Ag,Cu)InSe_2$ Solar Cells with KF Post-Deposition Treatment. *ACS Applied Energy Materials* **2021**, *4* (1), 233−241.

## ▥ Recommended by ACS

**Impacts of KF Post-Deposition Treatment on the Band Alignment of Epitaxial $Cu(In,Ga)Se_2$ Heterojunctions**

Takehiko Nagai, Norio Terada, *et al.*

APRIL 05, 2022
ACS APPLIED MATERIALS & INTERFACES    READ ☑

**Optical Detection of $SnSe_2$ Formation on CZTSSe Thin-Film Solar Cells**

Siwon Oh, Hyeonsik Cheong, *et al.*

AUGUST 24, 2022
ACS APPLIED ENERGY MATERIALS    READ ☑

**Synergetic Effects of Zn Alloying and Defect Engineering on Improving the CdS Buffer Layer of $Cu_2ZnSnS_4$ Solar Cells**

Liangli Chu, Chengyan Liu, *et al.*

JULY 27, 2022
INORGANIC CHEMISTRY    READ ☑

**Rear Interface Modification by the ZnTe Layer Enables High-Efficient $Cu_2(Zn,Cd)SnS_4$ Thin-Film Solar Cells**

Shijin Wang, Xudong Xiao, *et al.*

NOVEMBER 16, 2021
ACS APPLIED ENERGY MATERIALS    READ ☑

Get More Suggestions >